

Short Communication

Effects of Yb on the electrical and microstructural properties of $(Y_{1-x}Yb_x)Ba_2Cu_3O_{7-\delta}$ ($x = 0 - 1.0$) superconductor

A. N. Jannah^{1,2}, S. G. Thang², C. Kong², A. B. P. Ilhamsyah², S.K. Chen³,
R. Abd-Shukor^{2,*}

¹ Faculty of Applied Sciences, Universiti Teknologi MARA, Negeri Sembilan Branch, Kuala Pilah Campus, 72000, Kuala Pilah, Negeri Sembilan, Malaysia

² Department of Applied Physics, Universiti Kebangsaan Malaysia, Bangi, Selangor, Malaysia

³ Department of Physics, Universiti Putra Malaysia, Serdang 43400, Selangor, Malaysia

*E-mail: ras@ukm.edu.my

Received: 3 September 2020 / Accepted: 5 October 2020 / Published: 30 November 2020

The superconducting properties and the effects of Yb substitution on $(Y_{1-x}Yb_x)Ba_2Cu_3O_{7-\delta}$ (Y123) with $x = 0$ to 1.0 were investigated. The powder X-ray diffraction method, scanning electron microscopy and electrical resistance measurements were used to characterize the samples. All samples showed pure Y123 phase except for $x = 1$ which showed some impurity peaks. The lattice parameters and unit cell volume decreased as Yb content was increased indicating the smaller Yb^{3+} instead of the larger Yb^{2+} was substituted at the Y^{3+} site. The resistance-temperature curves showed metallic normal state behaviour in all samples. The superconducting transition temperature showed a slight decrease as Yb content was increased due to charge redistribution between the CuO chain and the CuO_2 plane as smaller Yb^{3+} replaced Y^{3+} . Our results showed that for Y123 type structure, the ionic radius of the rare-earth is more important than the valence state in forming a stable phase which can be superconducting or non-superconducting depending on the valence state of the rare earth ions. These results are useful in understanding the phase formation and transport mechanism of this material.

Keywords: microstructure; rare earths; x-ray diffraction; Yb-substitution

1. INTRODUCTION

The cuprate superconductors have been subjected to various substitutions and doping to probe the superconducting mechanism as well as to improve the physical properties. The properties of Bi-based and Tl-based cuprates have been reported to improve as a result of elemental substitutions and additions [1-3]. The $YBa_2Cu_3O_{7-\delta}$ (Y123) is an interesting material not only from the superconducting mechanism but also from the application point of view. It is highly adaptable chemically and has been subjected to a variety of cationic and anionic substitutions [4-13]. Many elements have been substituted into

YBa₂Cu₃O_{7-δ} and other superconductors, which provided useful information on the superconducting mechanism as well as methods to improve the physical properties for practical applications [14-16].

Yttrium in YBa₂Cu₃O_{7-δ} can be replaced with most of the rare earth elements (RE) and remains superconducting except for Ce, Tb and Pr. Ce and Tb cannot occupy the Y site and no REBa₂Cu₃O_{7-δ} phase can be formed. Pr on the other hand is able to replace Y and form the PrBa₂Cu₃O_{7-δ} phase but is not superconducting. Several works on the substitution of Pr for Y in YBa₂Cu₃O_{7-δ} have been performed to understand the suppression mechanism of superconductivity in this compound [6, 16, 17]. The ionic radii and valence state of the rare earths are important in the phase formation and superconductivity of the REBa₂Cu₃O_{7-δ} system. Some analysis showed that mixed valence Pr³⁺/Pr⁴⁺ is involved in the PrBa₂Cu₃O_{7-δ} compound. Pr⁴⁺ reduces the concentration of charge carrier (holes) to a level where superconductivity is totally suppressed resulting in a non-superconducting phase [6, 16]. The presence of mixed valence state of Pr in PrBa₂Cu₃O_{7-δ} has been shown experimentally through neutron-diffraction studies [17].

Yb is another element from the rare-earth family. Its unique property has made it applicable in many devices including optical fibre [18]. It is multivalent, Yb²⁺/Yb³⁺ and YbBa₂Cu₃O_{7-δ} has been shown to be superconducting. The ionic radius of Y³⁺ is 0.90 Å which is larger than Yb²⁺ (1.02 Å) but smaller than Yb³⁺ (0.868 Å) [19]. The ionic radius of Pr³⁺ is 0.99 Å and Pr⁴⁺ is 0.85 Å. Works on the substitution of Yb in Y_{1-x}Yb_xBa₂Cu₃O_{7-δ} for low levels ($x = 0$ to 0.15) has been reported [6]. X-ray diffraction shows that Yb³⁺ partly substitutes Y³⁺ site and the unit cell volume V decreases monotonically with increasing x . For this low-level substitution the transition temperature is between 90 and 91 K. In addition, the electron spin lattice relaxation (SLR) times of Yb³⁺ ions were measured from the temperature dependence of electron spin resonance line width in Y_{0.99}Yb_{0.01}Ba₂Cu₃O_y with different oxygen contents. The Debye temperature was found to increase with the transition temperature and oxygen contents y indicating phonons hardening tendency [20].

It is interesting to investigate further the effects of Yb on YBa₂Cu₃O_{7-δ} for $x > 0.15$. The complete transition from YBa₂Cu₃O_{7-δ} to YbBa₂Cu₃O_{7-δ} may give information about the role of ionic radius, valence state and crystal structure on the superconductivity of REBa₂Cu₃O_{7-δ} phase. In the case of Pr, both Pr³⁺ and Pr⁴⁺ are involved in the formation of the REBa₂Cu₃O_{7-δ} phase. Yb is also multivalent, Yb²⁺/Yb³⁺ and it is interesting to investigate the preferred valence state and ionic radius of Yb in (Y_{1-x}Yb_x)Ba₂Cu₃O_{7-δ}. In this paper we report results concerning changes in the superconducting and normal-state properties of polycrystalline (Y_{1-x}Yb_x)Ba₂Cu₃O_{7-δ} for $x = 0$ to 1.0. This work was also performed to determine which factor, ionic radius or valence state, is more important in the formation of Y123 and superconducting phase. X-ray diffraction patterns, Scanning Electron Microscope (SEM) micrographs together with the electrical resistance versus temperature results are presented.

2. MATERIALS AND METHODS

Samples with nominal compositions (Y_{1-x}Yb_x)Ba₂Cu₃O_{7-δ} for $x = 0, 0.2, 0.4, 0.5, 0.7, 0.9, 1.0$ were prepared by using the standard solid-state reaction technique. Appropriate amounts of high purity ($\geq 99.9\%$) Y₂O₃, Yb₂O₃, BaO and CuO powders were mixed and ground. The precursor powders were

calcined for 24 h at 900 °C and cooled to room temperature. The powders were reground and heated again at 900 °C for another 24 h. After furnace cooling, the powders were reground, pelletized (13mm diameter and 2 mm thickness), heated at 900 °C for 24 h, and cooled to room temperature at around 1°C/min.

The samples were analyzed by powder X-ray diffraction method using a Siemens D-5000 diffractometer with Cu-K α source from $2\theta = 0$ to 60° to identify the resultant phases. The lattice parameters were calculated by using the least squares fitting method with at least 10 peaks. A variable Pressure Scanning Electron Microscope (LEO-VPSEM) was used to determine the microstructure of the samples. ImageJ software employing 50 grains was used to determine the average grain size.

The dc electrical resistance measurements were performed using the four-probe method. Silver pastes were used as electrical contacts. The experimental set-up consists of Keithley 220 Programmable Current Source and Keithley 197 Autoranging Microvolt DMM. A constant current from 1 mA to 100 mA was used throughout the measurements. A closed cycle refrigerator from CTI Cryogenics Closed Cycle Refrigerator Model 22 and a temperature controller from Lakeshore Temperature Controller Model 325 were used for low temperature measurements.

3. RESULTS AND DISCUSSION

The XRD patterns of $(Y_{1-x}Yb_x)Ba_2Cu_3O_{7-\delta}$ are presented in Figure 1(a) for $x = 0, 0.2, 0.4$ and 0.5 , and Figure 1(b) for $x = 0.7, 0.9$ and 1.0 . Diffraction lines of all samples showed $(Y_{1-x}Yb_x)Ba_2Cu_3O_{7-\delta}$ phase with layered orthorhombic perovskite Y123 structure (with Pmmm space group). The XRD patterns showed no impurity phase for samples with $x = 0 - 0.9$.

However, some impurity phases were observed in $x = 1.0$ (Figure 1(b)) which included $(Y/Yb)_2BaCuO_y$ (Y211) and $BaCuO_2$. Table 1 shows the lattice parameters, unit cell volume, orthorhombicity ε , onset-transition temperature, $T_{c-onset}$, zero-resistance temperature, T_{c-zero} and transition-width (ΔT_c) of $(Y_{1-x}Yb_x)Ba_2Cu_3O_{7-\delta}$. As Yb was increased, the lattice parameters a , b and c and unit cell volume decreased (Figure 2) indicating the incorporation of Yb in the $(Y_{1-x}Yb_x)Ba_2Cu_3O_{7-\delta}$ structure. Yb has two valence states, Yb^{2+} with ionic radius 1.02 Å and Yb^{3+} with ionic radius 0.868 Å. The decrease in the lattice parameters indicated the substitution of smaller Yb^{3+} into Y^{3+} with ionic radius 0.90 Å. Hence in this system the smaller Yb^{3+} was preferred over the larger Yb^{2+} for substitution at the Y site. The orthorhombicity $\varepsilon = \frac{a-b}{a+b}$ for $Y_{1-x}Yb_xBa_2Cu_3O_{7-\delta}$ was around $8.6 - 9.4 \times 10^{-3}$ (Table 1) with no systematic change among the samples. The orthorhombic structure was preserved.

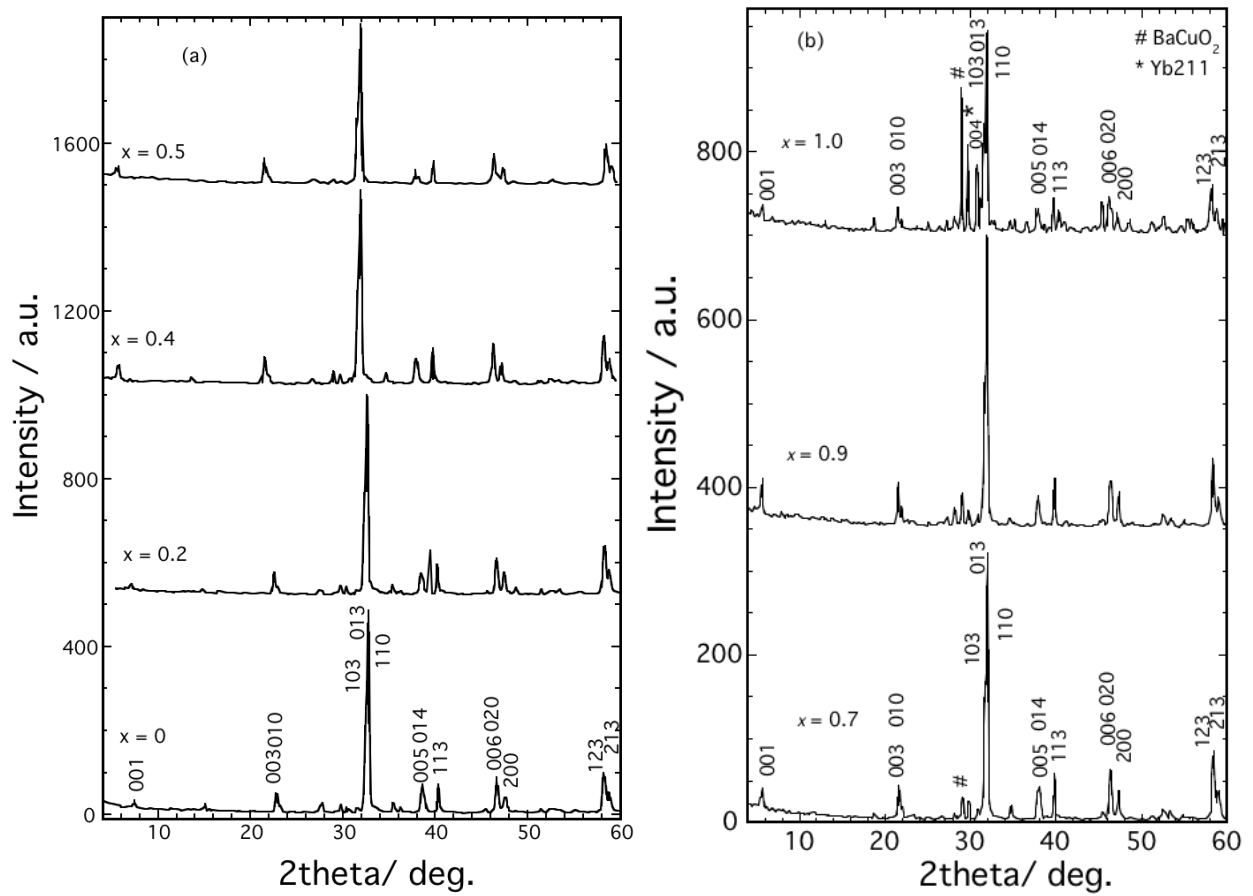


Figure 1. Powder X-ray diffraction patterns of $(Y_{1-x}Yb_x)Ba_2Cu_3O_{7-\delta}$ for (a) $x = 0, 0.2, 0.4, 0.5$ and (b) $x = 0.7, 0.9, 1.0$. Impurities: # - $BaCuO_2$ and * - Yb_2O_3 .

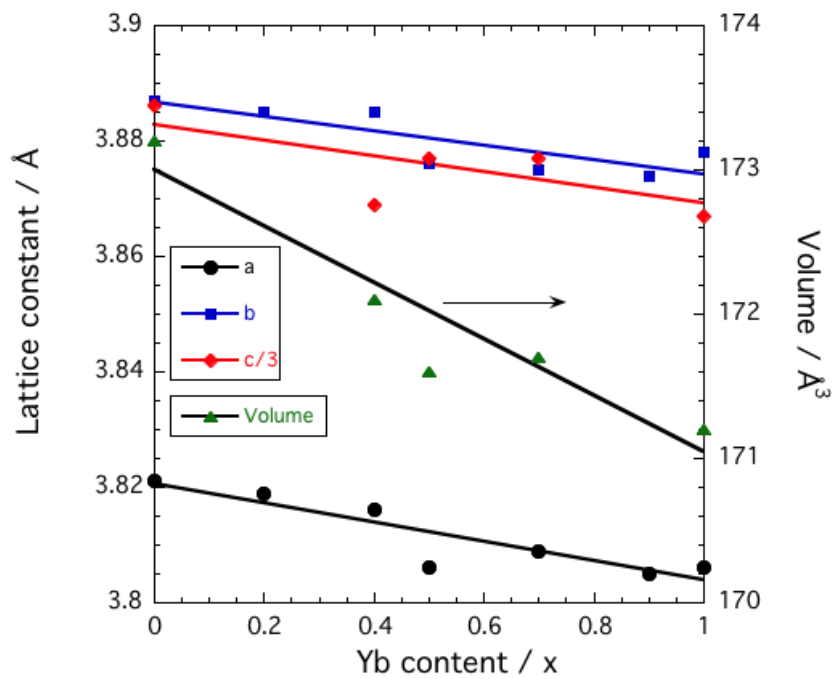
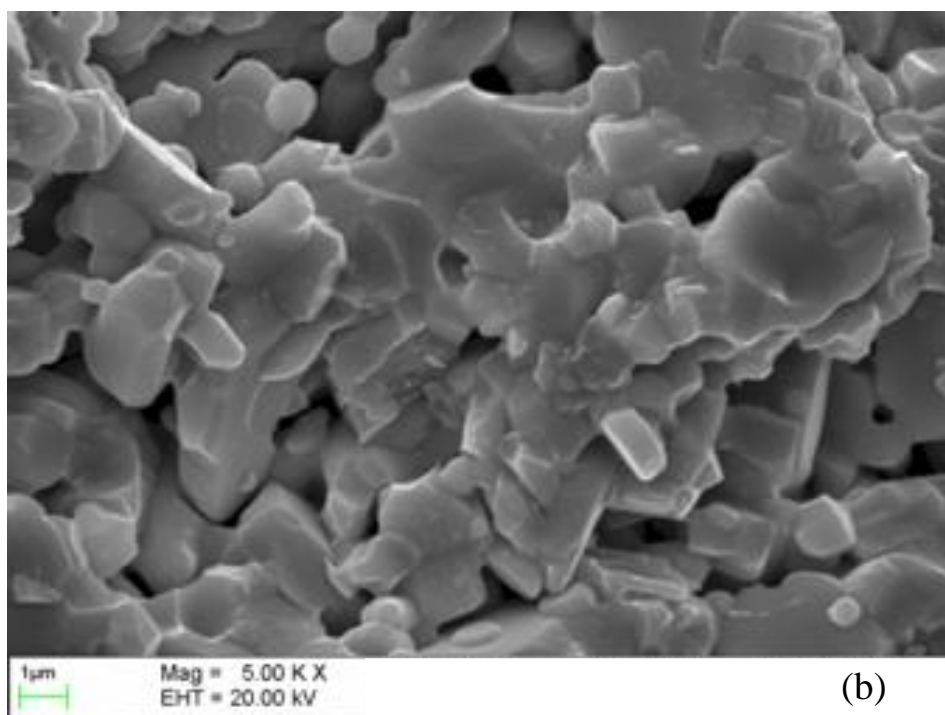
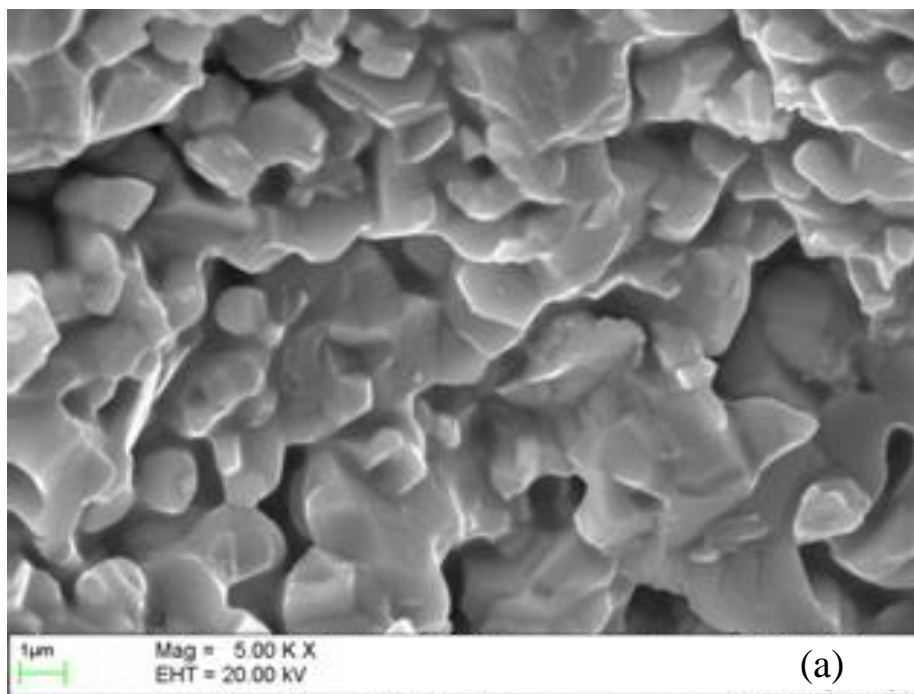
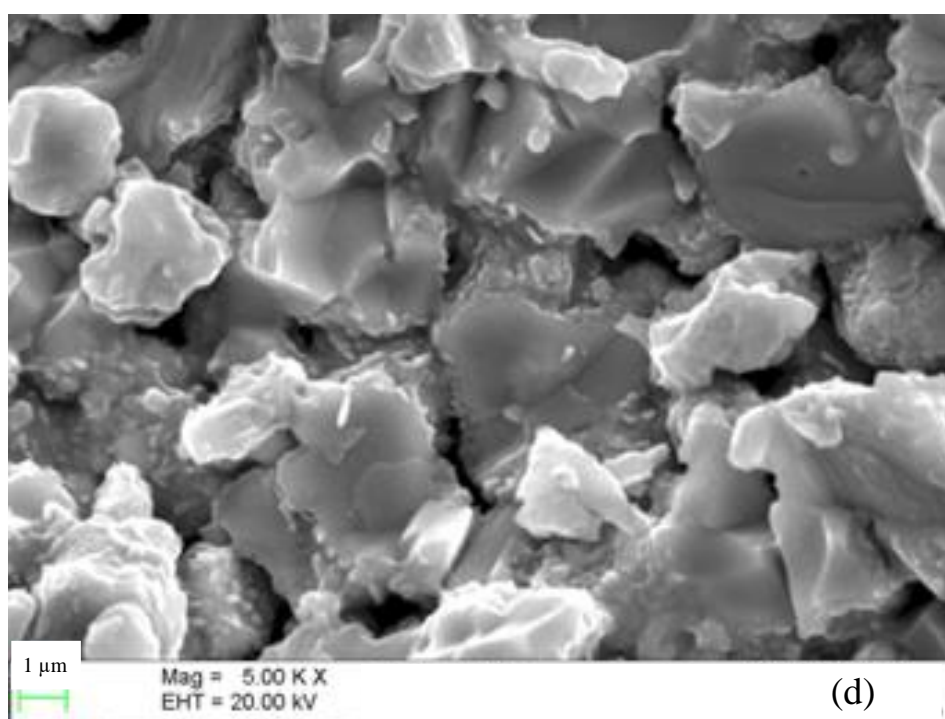
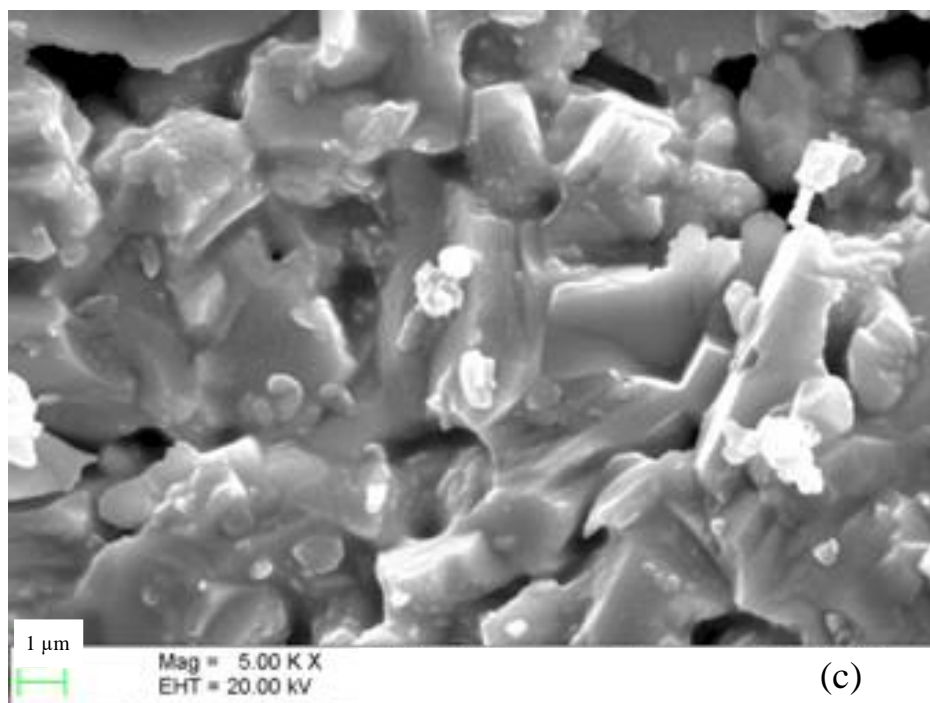


Figure 2. Lattice parameters and unit cell volume versus x for $(Y_{1-x}Yb_x)Ba_2Cu_3O_{7-\delta}$





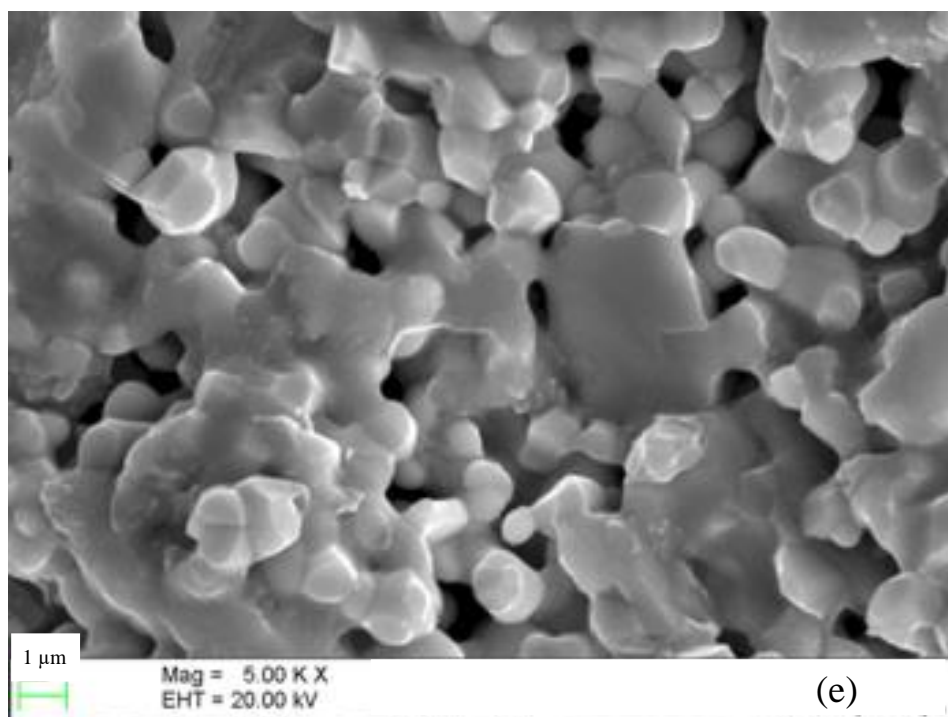
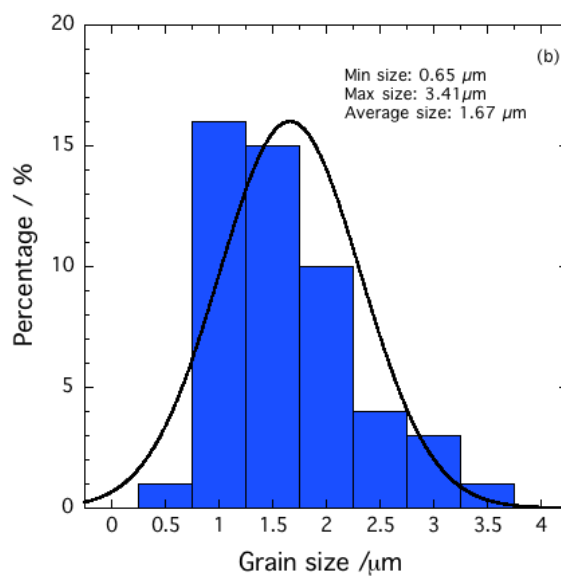
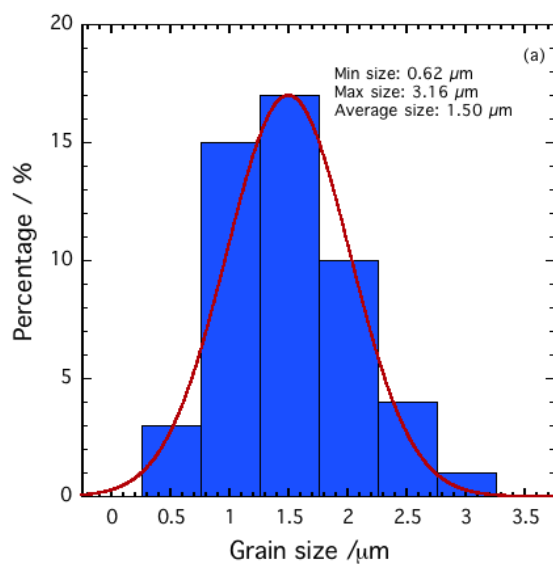


Figure 3. Scanning electron micrographs of $(Y_{1-x}Yb_x)Ba_2Cu_3O_{7-\delta}$ for (a) $x = 0$, (b) $x = 0.2$, (c) $x = 0.5$, (d) $x = 0.7$, (e) $x = 1.0$



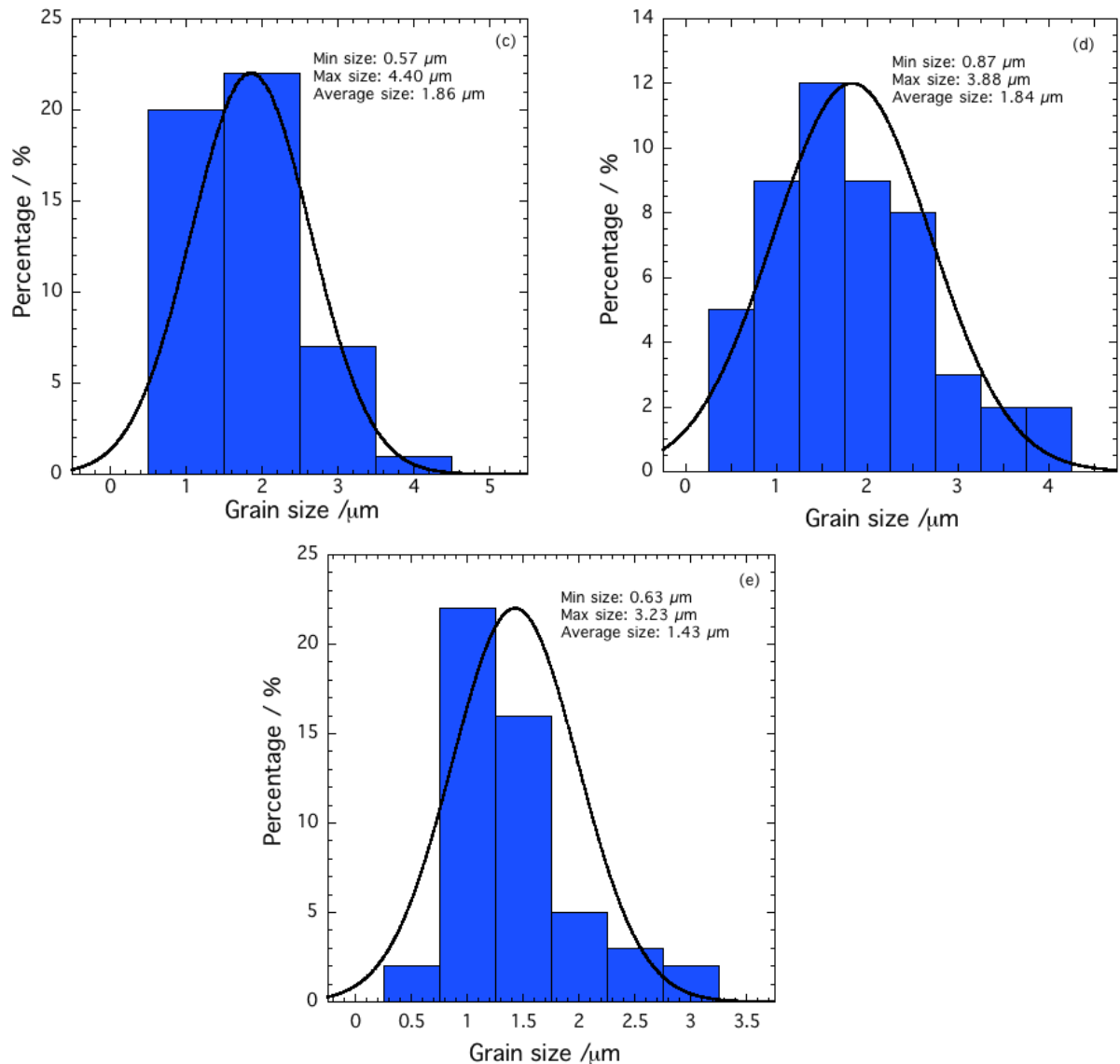


Figure 4. Histogram of grain size distribution of $(Y_{1-x}Yb_x)Ba_2Cu_3O_{7-\delta}$ for (a) $x = 0$, (b) $x = 0.2$, (c) $x = 0.5$, (d) $x = 0.7$ and (e) $x = 1.0$.

Figures 3(a) – 3(e) show the SEM micrographs for $x = 0, 0.2, 0.5, 0.7$ and 1.0 . The histograms for the grain size are shown in Figure 4. The histograms shows that the average grain size increased slightly with increasing Yb content starting from $x = 0$ to $x = 0.5$. The average grain size for $x = 0$ was $1.50 \mu\text{m}$ while the average grain size for $x = 0.5$ was $1.86 \mu\text{m}$. The average grain size for $x = 1.0$ was $1.43 \mu\text{m}$.

The electrical resistance versus temperature curves of $(Y_{1-x}Yb_x)Ba_2Cu_3O_{7-\delta}$ are shown in Figure 5 (a) for $x = 0, 0.2, 0.4, 0.5$ and (b) for $x = 0.7, 0.9$ and 1.0 . All samples exhibited a metallic normal state behaviour above the transition temperature. $T_{c\text{-onset}}$ was 91 K and $T_{c\text{-zero}}$ was 89 K for the $x = 0$ samples. In order to determine the general trend of the transition temperatures, the data were fitted with a simple linear model. The fits showed that the transition temperature especially $T_{c\text{-zero}}$ decreased slightly as the amount of Yb was increased from $x = 0$ to 1 (Figure 6).

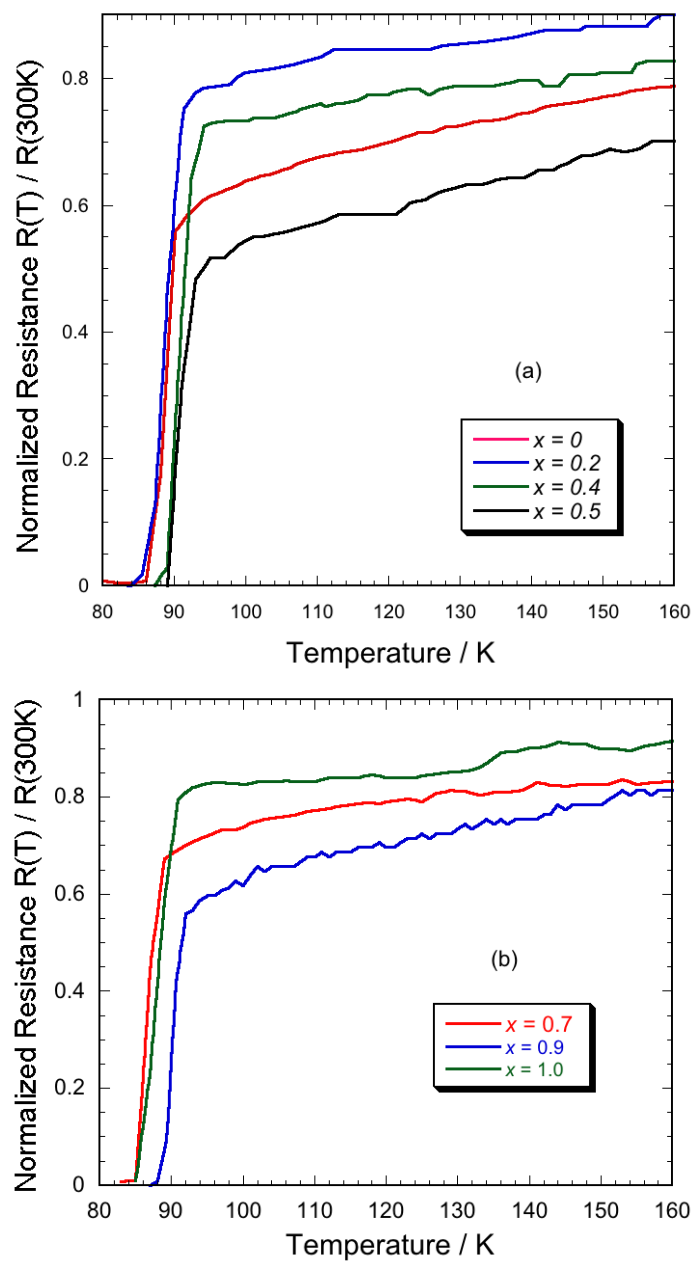


Figure 5. Electrical resistance temperature dependence of $(Y_{1-x}Yb_x)Ba_2Cu_3O_{7-\delta}$ for (a) $x = 0, 0.2, 0.4, 0.5$ and (b) $x = 0.7, 0.9, 1.0$.

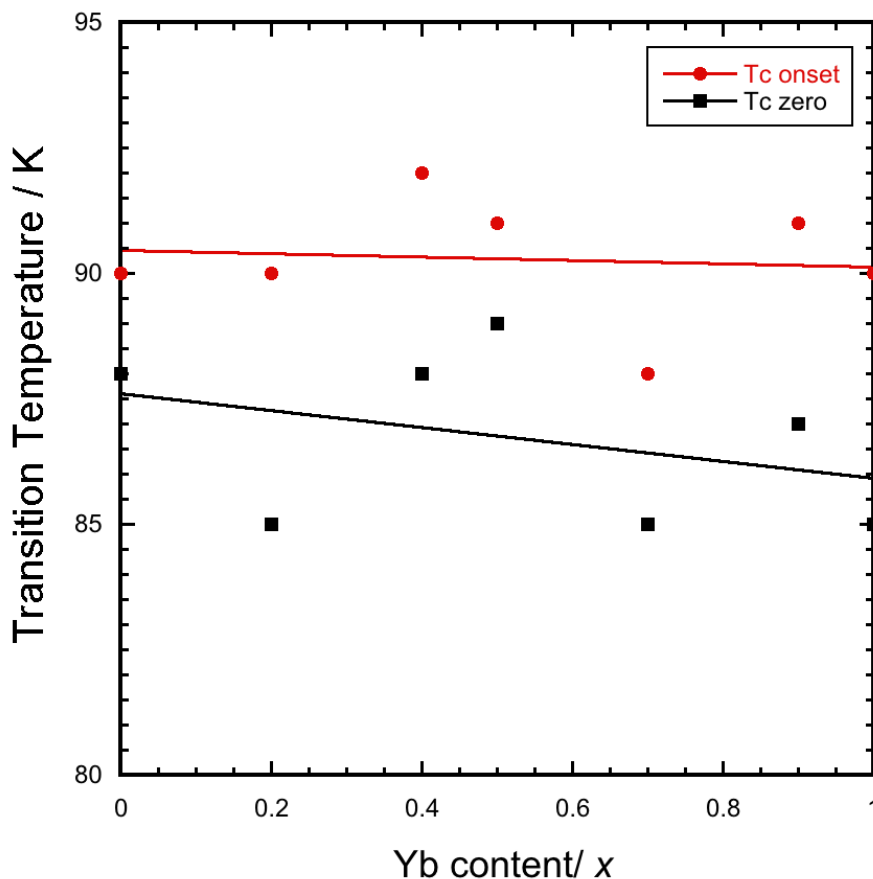


Figure 6. The variation of T_{c-zero} and $T_{c-onset}$ as a function of x for $(Y_{1-x}Yb_x)Ba_2Cu_3O_{7-\delta}$. The solid lines are linear fits that show a decreasing trend in the transition temperature.

It is generally known that as the ionic radius of the rare-earth is decreased the transition temperature also decreased [21, 22]. This shows that the carrier concentration increased with decreasing ionic radius and $REBa_2Cu_3O_{7-\delta}$ becomes over-doped. These changes were suggested to be due to strain-induced charge redistribution between the CuO chain and the CuO₂ plane, which is caused by the substitution of small RE ions [21]. This is consistent with the increase in the Debye temperature [20] which indicates phonons hardening as Yb substituted Y due to the reduction in the lattice parameters and unit cell volume. The $x = 1$ samples showed a much reduced T_{c-zero} (85 K) and this may be attributed to the presence of impurities such as Yb211 and BaCuO₂. The preparation method of pure $YbBa_2Cu_3O_{7-\delta}$ is not the same as $YBa_2Cu_3O_{7-\delta}$ as reported by Sato et al. [8]. However the $x = 0.9$ samples showed a single Y123 phase. These results showed that a single phase could be obtained with a small amount of Y in $YbBa_2Cu_3O_{7-\delta}$.

We now compare the effects of Yb and Pr substitutions in $(Y_{1-x}RE_x)Ba_2Cu_3O_{7-\delta}$. In terms of ionic radius, Pr^{3+} is within 10% of the ionic radius of Y^{3+} while Pr^{4+} is within 3%. The ionic radius of Yb^{2+} is within 13% of Y^{3+} while Yb^{3+} is within 3.6%. One reason why Yb was chosen for this study is because it is multivalent and Y^{2+} has ionic radius, which is very similar to other rare earths, such as Gd^{3+} (0.938 Å) and La^{3+} (1.032 Å), which show the superconducting phase. Although in principle Yb^{2+} can be easily accommodated in the Y123 structure, the system prefers the Yb^{3+} state because this is much closer to the ionic radius of Y^{3+} . These results showed that the ionic radius of the rare earth is more

important than the valence state in forming the REBa₂Cu₃O_{7-δ} phase.

In conclusions, we have studied the effects of Yb on the superconducting properties of (Y_{1-x}Yb_x)Ba₂Cu₃O_{7-δ} for $x = 0$ to 1.0. Pure Y123 type structure can be formed until $x = 0.9$. The lattice parameters decreased with increase in Yb substitution indicating the substitution of Yb³⁺ in place of Y³⁺. Strain-induced charge redistribution between the CuO chain and the CuO₂ plane resulted in the slight decrease in T_c as result of smaller Yb³⁺ substitution in place of Y³⁺. This work showed that the radius of the rare earth ions is more important than their valence states in forming the Y123 type structure. Further works on other multivalent rare earth substitution can be useful in understanding the transport properties of this material.

Table 1. Lattice parameters a , b , c , unit cell volume V , orthorhombicity ε , onset temperature $T_{c\text{-onset}}$, zero-resistance temperature, $T_{c\text{-zero}}$ and transition-width, ΔT_c of (Y_{1-x}Yb_x)Ba₂Cu₃O_{7-δ}

x	$a / \text{\AA}$	$b / \text{\AA}$	$c / \text{\AA}$	$V / \text{\AA}^3$	ε	$T_{c\text{-onset}} / \text{K}$	$T_{c\text{-zero}} / \text{K}$	$\Delta T_c / \text{K}$	Grain size / μm
0.0	3.821	3.887	11.660	173.2	8.6	91	89	2	1.50
0.2	3.819	3.885	11.640	172.7	9.0	90	85	5	1.67
0.4	3.816	3.885	11.606	172.1	8.8	92	88	4	-
0.5	3.806	3.876	11.630	171.6	8.6	91	89	2	1.86
0.7	3.809	3.875	11.630	171.7	8.6	89	85	6	1.84
0.9	3.805	3.874	11.620	171.3	9.0	91	87	4	-
1.0	3.806	3.878	11.600	171.2	9.4	90	85	5	1.43

ACKNOWLEDGMENTS

The research was funded by the Ministry of Higher Education, Malaysia under grant number FRGS/2017/STG02/UKM/01/1. A. N. Jannah thanks UiTM and Ministry of Higher Education, Malaysia for the post-doctoral grant.

References

1. Abdullah Aljaafari, A. Sedky and Ayman Al- Sawalha, *J. Phys. & Chem. Sol.*, 69 (2008) 2919.
2. A.I. Abou Aly, I.H. Ibrahim, R. Awad, A. El-Harizy and A. Khalaf, *J. Supercond. Nov. Magn.*, 23 (2010) 1325.
3. K. Muhammad-Aizat and R. Abd-Shukor, *Sains Malaysiana*, 47(7) (2018) 1579.
4. Annas Al-Sharabi, Sarah Yasmin Tajuddin, Au Diya Fatihah Wan Saffiey, Syazana Jasman, H.A. Alwi, M.H. Jumali and R. Abd-Shukor, *Sains Malaysiana*, 45 (2016) 1959.
5. Kong Wei, Kong Ing, M. S. Hamdan, S. Radiman and R. Abd-Shukor, *J. Supercond. and Nov. Mag.*, 31(9) (2018) 2699.
6. X. Sheng, G. Yangni and W. Xiaoshan, *J. Rare Earths*, 28 (2010) 431.
7. Z. Homonnay, Z. Klencsar, V. Chechersky, Gy. Vankó, M. Gál, E. Kuzmann, S. Tyagi, J-L. Peng,

- R. L. Greene and A. Vértes, *Phys. Rev. B*, 59 (1999) 11596.
8. Y. Sato, V. Petrykin, H. Yasuoka and M. Kakihana, *J. Ceram. Soc. Jpn.*, 120 (2012) 503.
 9. Y. Slimani, M.A. Almessiere, E. Hannachi, M. Mumtaz, A. Manikandan, A. Baykal and F. Ben Azzouz, *Ceram. Int.*, 45 (2019) 6828.
 10. R.K. Singhal, *Mat. Lett.*, 65 (2011) 825.
 11. V.N. Vieira, P. Pureur, J. Schaf, *Phys. C*, 353 (2001) 241.
 12. L. Zhang, L. P. Yu, W. Zhang, Y. Z. Wang, H. Zhang and Y. Zhao, *Physica C*, 357 (2001) 194.
 13. S. Dadras, S. Dehghani, M. Davoudiniya and S. Falahati, *Mater. Chem. Phys.*, 193 (2017) 496.
 14. A.I. Abou-Aly, R. Awad, I.H. Ibrahim and W. Abdeen, *Solid State Commun.*, 149 (2009) 281.
 15. M. Almessiere, Y. Slimani, E. Hannachi, R. Algarni and F. Ben Azzouz, *J. Mater. Sci. - Mater. Electron.*, 30 (2019) 17572.
 16. R. Fehrenbacher, T. M. Rice, *Phys. Rev. Lett.*, 70 (1993) 3471.
 17. M. Guillaume, P. Allenspach, W. Henggeler, J. Mesot, B. Roessli, U. Staub, P. Fischer, A. Furrer and D. Trounov, *J. Phys.: Condens. Mat.*, 6 (1994) 7963.
 18. M. A. M. Salim, M. Z. A. Razak, S. R. Azzuhri, M. A. Ismail, F. Ahmad and S. W. Harun, *Sains Malaysiana*, 48 (2019) 1289.
 19. R.D. Shannon, *Acta Cryst.*, 32 (1976) 751.
 20. L. K. Aminov, V. A. Ivanshina, I.N. Kurkin, M. R. Gafurova, I. Kh. Salikhov, H. Keller and M. Gutmann, *Physica C*, 349 (2001) 30.
 21. J.G. Lin, C.Y. Huang, Y.Y. Xue, C.W. Chu, X.W. Cao and J. C. Ho, *Phys. Rev. B*, 51 (1995) 12900.
 22. S. V. Samoylenkov, O. Yu. Gorbenko and A. R. Kaul, *Physica C*, 278 (1997) 49